Proceedings of IMECE2005
2005 ASME International Mechanical Engineering Congress and Exposition
November 5-11, 2005, Orlando, Florida USA

IMECE2005-82282

CONTROL OF CYLINDRICAL SHELL PANELS WITH INPUT SHAPING AND PHASE SHIFT OF SHAPE MEMORY RING SEGMENTS

J.G. DeHaven and H.S. Tzou
Department of Mechanical Engineering,
Structronics and Design Lab.
University of Kentucky, Lexington, KY 40506-0503
Email: hstzou@engr.uky.edu

ABSTRACT

The purpose of this study is to investigate the control effect from shape memory alloy (SMA) ring segments placed at the desired positions along the length of a cylindrical shell panel. Equations of motion for an elastic cylindrical shell panel are defined first and then used with the assumed mode shape functions for the appropriate boundary conditions in a free vibration analysis. The results from this are used with the generic shell sensing equation to determine the spatial strain distribution. From this, optimal placement of ring segments for each given mnth mode is determined. Through use of the modal expansion method, the open-loop control force induced by the SMA ring segments applied to a cylindrical shell panel is determined next. This evaluation shows that only the odd modes in the circumferential direction can be controlled. Longitudinal modes are controlled via placing a varying number, depending on the mode, of ring segments along the length of the cylindrical shell panel. To predict control effects of the SMA ring segments, the modal participation factor response is determined for an external harmonic excitation applied to the shell along with SMA control force induced to eliminate the unwanted effects. The results show that with proper choice of waveform function for the applied temperature to the SMA ring segments and minor modifications to frequency and phase, the SMA ring segments can control unwanted external vibration.

INTRODUCTION

There have been a variety of disciplines and fields which have employed the use of smart materials to create active systems which can sense changes in the environment and make modifications when and where they are needed. Shape memory alloys (SMAs) have become a popular material to use in such systems because of the large forces and deformations generated during phase transformation and its excellent recovery of large strains. Researchers in biomedical engineering have used SMAs to design stents for opening constricted blood vessels and active catheters for easier navigation of blood vessels and thus reducing pain inflicted upon patients (Lee and Lee, 2000; Mineta, et al., 2002). Research in biomimetics has produced active hydrofoils which are controlled via shape memory wires that actuate sections of the hydrofoil for generating propulsion similar to a fish (Rediniotis et al. 1998). There have also been a number of developments generated by trying to create shape changing airfoils which would allow altering the aerodynamic characteristics for enhanced performance within different flight regimes, one of these designs involved using shape memory alloy torque tubes in the DARPA / Wright Lab "Smart Wing" (Kudva, et al., 1997). Many researchers have investigated position and tracking control with shape memory wires and springs (Madill and Wang 1998; Ma, et al., 2003; Majima, et al., 2001). Shape memory alloys have been embedded within a number of composite materials for a variety of purposes including reducing hoop stress within high-pressure vessels, active vibration and structural acoustic control through active strain energy tuning (ASET) and/or active modal modification, shape control of composite beams, and control of wave propagation in rods (Paine, et al., 1995; Rogers, 1990; Jia and Rogers, 1990; Baz, et al., 2000; Chen, et al., 2000). The use of shape memory alloys for controlling the clearance between the shroud and tip of the blade within the

high pressure turbine of a turbine engine is also being looked at because of the major benefits resulting from keeping the clearance gap at a constant minimum and the difficulty of doing so caused by several mechanisms including centrifugal and aerodynamic loads and the non-uniform thermal expansion/contraction of numerous parts (Schetky and Steinetz, 1998; Lattime and Steinetz, 2002).

There are several classifications associated with the shape memory effect, the three most common are 1) the one-way effect, 2) the two-way effect, and 3) the pseudoelastic effect. The shape memory effect was first discovered in a gold-cadmium (AuCd) alloy by Chang and Read (1951), since then it has been found in a number of other materials including the nickel titanium (NiTi) alloys introduced by Buehler et al. who were working for the Naval Ordinance Laboratory from which the alloy is commonly named Nitinol (1963). SMAs are known for their phase transformations from austenite to martensite and vice versa within their working temperature range which create their unique thermomechanical properties. The one-way effect generally involves loading the material in the martensite phase such that large plastic deformation occurs, typically 5 to 8% for NiTi alloys, removing the load and then applying heat in some form such that the temperature of the material goes above the austenite transformation temperature range. This causes the material to return to its original shape, recovering all the induced strain via a phase transformation. The two-way effect is used more often than the one-way effect due to its appropriate nature for use in actuators. Here the SMA is typically loaded in the martensite phase to produce large deformation and heated without removing the load generating large stresses, caused by transformation to austenite which generally for NiTi alloys has a 2 to 3 times stiffer elasticity than its martensite phase, thus forcing the SMA to try and return to its approximate original shape with lower strain than in the corresponding martensite phase. Next the SMA is cooled causing another phase transformation back to martensite and returning to the original large deformation caused by the applied load. This process may be cycled a number of times as required by actuators but the amount of plastic deformation caused in the martensitic phase must be less than that the maximum allowed due to possible failure caused by fatigue. The pseudoelastic effect occurs when the SMA is already in the austenite phase just above the austenite finish temperature and loaded such that there is a stress induced transformation to martensite allowing for large deformation. Then once the stress is removed the SMA returns to its original geometry since the material temperature is already above the austenite transition region.

The main objective of this research is to evaluate the possibility of using shape memory alloys for controlling the static deflection and vibration of cylindrical shells applied to turbine engine control. Shape memory alloys were chosen because of their ability to generate large forces as previously mentioned. This ability is very desirable for cases where the shell is relatively stiff and static deflection may be more important than the vibration control. While the current shape memory alloys are not as practical for vibration control because of their inability to be cycled at high frequencies, this may change depending on the type of heating and cooling employed and the use of other chemical compositions resulting in different shape memory alloys with different abilities. The approach to solving the problems involved with vibration is to place shape memory rings, which could be SMA wire or ribbon, along the length of the cylindrical shell in positions where the strain resulting from vibration is highest. To determine these locations a sensing analysis, based on use of piezoelectric sensors, for different modes is performed. The SMA rings were modeled as being elastically stretched in the martensite phase and positioned on the shell. These rings would be actuated and the resulting force would be applied normal to the shell surface. No plastic deformation of the SMA occurs so there will not be any large strains to recover, yet because the stiffness of the SMA increases by 2 to 3 times during transformation to austenite, large forces can be generated. The actuation of the SMA rings is modeled as linear in one dimension (1D). The SMA force is used in a forced vibration analysis to determine whether or not it can control the vibration of various cylindrical shell geometries.

SMA FORCES DEFINED IN EQUATIONS OF MOTION FOR CYLINDRICAL SHELL PANELS

In order to determine how to control a cylindrical shell panel with a shape memory ring segment, the way the SMA force is defined in the equations of motion for a cylindrical shell panel must be evaluated first. The equations of motion for a cylindrical shell panel can be written as (Tzou, 1993)

$$\frac{\partial N_{xx}^{m}}{\partial x}+\frac{1}{R}\frac{\partial N_{\psi x}^{m}}{\partial \psi}+q_{x}-\rho h\ddot{u}_{x}=0 \tag{1}$$

$$\frac{\partial N_{x\psi}^{m}}{\partial x}+\frac{1}{R}\frac{\partial N_{\psi\psi}}{\partial \psi}+\frac{1}{R}\frac{\partial M_{x\psi}^{m}}{\partial x}+\frac{1}{R^{2}}\frac{\partial M_{\psi\psi}}{\partial \psi}+q_{\psi}-\rho h\ddot{u}_{\psi}=0 \tag{2}$$

$$\frac{\partial^{2} M_{xx}^{m}}{\partial x^{2}}+\frac{2}{R}\frac{\partial^{2} M_{x\psi}^{m}}{\partial \psi^{2}}+\frac{1}{R^{2}}\frac{\partial^{2} M_{\psi\psi}}{\partial \psi^{2}}-\frac{N_{\psi\psi}}{R}+q_{3}-\rho h\ddot{u}_{3}=0 \tag{3}$$

The N_{ij} and M_{ij} are defined as the membrane force per unit length and the bending moment per unit length respectively. Those terms with the superscript m are defined as being only mechanical forces and moments, while those without superscripts $N_{\psi\psi}$ and $M_{\psi\psi}$ contain both mechanical loads, superscript m, and loads from the actuating force, superscript a (here the actuating force is from the SMA). $N_{\psi\psi}$ and $M_{\psi\psi}$ are defined below as

$$N_{\psi\psi}=N_{\psi\psi}^{m}-N_{\psi\psi}^{a} \tag{4}$$

$$M_{\psi\psi} = M^{m}_{\psi\psi} - M^{a}_{\psi\psi} \tag{5}$$

The reason for $N_{\psi\psi}$ and $M_{\psi\psi}$ containing the actuating force components is due to the way the SMA ring segments are fitted to the cylindrical shell panel. These SMA ring segments consist of wires or ribbons that run across the cylindrical shell panel circumferentially and their number and placement along the length is determined by the modes that are trying to be controlled, or in other words they are placed in the regions of highest strain based on the neural signals from a modal analysis, for detailed plots of these signal distributions see DeHaven et al. (2005). Figure 1 shows the placement and orientation of these SMA ring segments.

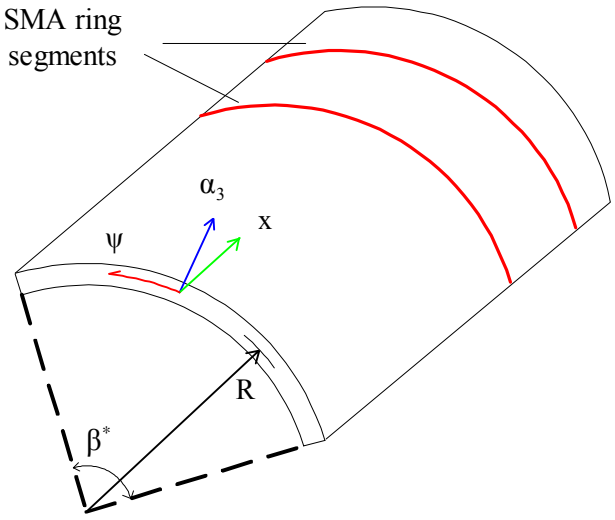

Figure 1 Cylindrical shell panel with SMA ring segments

The SMA ring segments are to be stretched in the martensite phase to a certain percent strain that is below the yield strain of martensite and attached to the shell at the simply supported boundaries. When these SMA wires or ribbons are heated above the austenite start and finish temperatures the phase transition to austenite will occur. The SMA will try to recover this strain even though no apparent detwinning (occurs when strain is generated beyond the martensite yield limit) of the martensite variants have occurred. The SMA wire will try to constrict and assuming the shell is sufficiently rigid will not be able to recover much of this strain, thus causing the forces and bending moments in the circumferential direction represented by $N_{\psi\psi}$ and $M_{\psi\psi}$.

A single SMA ring segment is designed to control the circumferential modes (the oscillations running the circumference of the shell and related to the mode number n of the (m,n) mode) and multiple ring segments are used in order to control the longitudinal modes (the oscillations running the length of the shell and related to the mode number m of the (m,n) mode). For example, based on the results from DeHaven et al. (2005), in order to control the (1,1) mode, one SMA segment is needed and it should be placed at the half way point along the length (x-direction) of the shell, **Figure 2**; or in order to control the (2,3) mode, two SMA segments are needed and should be placed at the one fourth and three fourths positions along the length of the shell, **Figure 3**.

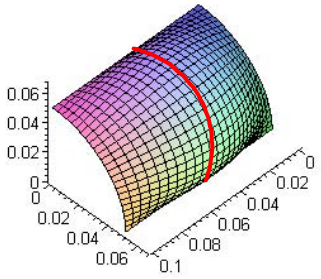

Figure 2 Neural signal distribution based on (1,1) mode of 90° cylindrical shell panel, red line is SMA ring segment placed at the half way point along the length of the shell

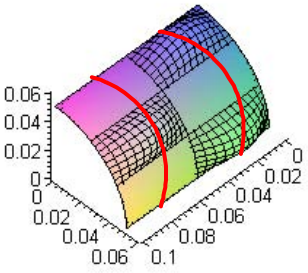

Figure 3 Neural signal distribution based on (2,3) mode of 90° cylindrical shell panel, red lines denote SMA ring segments placed at the one fourth and three fourths positions along the length of the shell

Since deflections normal to the shell are much more significant than deflections in the in-plane directions, the transverse equation (3) is only considered in future analysis. Assuming no other external influences (q_3=0) and substituting equations 4 and 5 into equation 3, it becomes

$$\frac{\partial^2 M^{m}_{xx}}{\partial x^2} + \frac{2}{R}\frac{\partial^2 M^{m}_{x\psi}}{\partial \psi^2} + \frac{1}{R^2}\frac{\partial^2 \left(M^{m}_{\psi\psi} - M^{a}_{\psi\psi}\right)}{\partial \psi^2} - \frac{\left(N^{m}_{\psi\psi} - N^{a}_{\psi\psi}\right)}{R} - \rho h \ddot{u}_3 = 0 \tag{6}$$

Equation 6 can be rearranged as follows and leaves the terms in brackets to be labeled as Q_3 which will be used later in the next section for the forced harmonic analysis.

$$\frac{\partial^2 M^m_{xx}}{\partial x^2}+\frac{2}{R}\frac{\partial^2 M^m_{x\psi}}{\partial \psi^2}+\frac{1}{R^2}\frac{\partial^2 M^m_{\psi\psi}}{\partial \psi^2}-\frac{N^m_{\psi\psi}}{R} + \left[\frac{N^a_{\psi\psi}}{R}-\frac{1}{R^2}\frac{\partial M^a_{\psi\psi}}{\partial \psi^2}\right]-\rho h\ddot{u}_3=0 \quad (7a)$$

$$Q_3=\frac{N^a_{\psi\psi}}{R}-\frac{1}{R^2}\frac{\partial M^a_{\psi\psi}}{\partial \psi^2} \quad (7b)$$

Based on the one dimensional (1D) two way shape memory effect the constitutive equation can be written in terms of stress T, strain S, elastic modulus Y, and martensite volume fraction ξ (Madill and Wang, 1998)

$$T=\begin{cases}[Y_A-(Y_A-Y_M)\xi]S & 0\le S<S^y_M \\ [Y_A-(Y_A-Y_t)\xi]S+\xi(Y_t-Y_M)S^y_M & S^y_M\le S<S^d_M \\ [Y_A-(Y_A-Y_d)\xi]S+\xi(Y_t-Y_M)S^y_M+(Y_d-Y_t)S^d_M & S^d_M<S\end{cases} \quad (8)$$

where subscripts M, A, t, and d stand for martensite, austenite, twinned and detwinned martensite respectively. The strains at specific points on the stress strain curve S^y_M and S^d_M stand for the yield strain of twinned martensite and the minimum strain of detwinned martensite respectively. The martensite volume fraction describes the amount of martensite present within the shape memory material at a given moment; it is defined as a number between 0 and 1, 1 being 100% martensite and 0 being 0% martensite or 100% austenite. The transformation kinetics governing the evolution of the martensite volume fraction ξ are given by Dutta et al. (2004) and defines the martensite volume fraction only as a function of temperature θ:

$$\frac{d\xi}{d\theta}=\begin{cases}\dfrac{1-\xi-h_-(\theta)}{h_-(\theta)-h_+(\theta)}g_+(\theta) & \dot{\theta}\ge 0 \\ \dfrac{h_+(\theta)+\xi-1}{h_-(\theta)-h_+(\theta)}g_-(\theta) & \dot{\theta}<0\end{cases} \quad (9a)$$

The initial condition for the differential equation is $\xi(0) = 1$. The functions g and h are given by Gaussian probability distribution functions (PDFs) and error functions.

$$g_{+/-}(\theta)=\frac{1}{v_{+/-}\sqrt{2\pi}}\exp\left(-\frac{(\theta-m_{+/-})^2}{2v^2_{+/-}}\right) \quad (9b)$$

$$h_{+/-}(\theta)=\frac{1}{2}\left[1+\mathrm{erf}\left(\frac{\theta-m_{+/-}}{v_{+/-}\sqrt{2}}\right)\right] \quad (9c)$$

These functions are characterized by the mean $m_{+/-}$ and the standard of deviation $v_{+/-}$, where the values for these are based on transformation temperatures of the shape memory alloy; the +/- subscripts stand for increasing and decreasing curves respectively. $N_{\psi\psi}$ and $M_{\psi\psi}$ can be defined in terms of the SMA force per unit length and bending moment per unit length respectively, using the constitutive equation (8) and transformation kinetics for the martensite volume fraction ξ (equation 9).

$$N^a_{\psi\psi}=Y_sSw \quad (10)$$

$$M^a_{\psi\psi}=r^a_\psi Y_sSw \quad (11)$$

S is the 1D strain in the martensite phase for the SMA ring segment, w is the width of the SMA ring segment, Y_s is the elastic modulus for the SMA where it is defined as

$$Y_s=[Y_A-(Y_A-Y_M)\xi] \quad (12)$$

r^a_ψ is the bending moment arm in the ψ direction (distances measured from the neutral surface of the shell to the mid-surface of the actuator). A constant strain value S will be used as an approximation because it is really dependent on the shell behavior. If the shell is very flexible, like being made of thin rubber, very little force will be applied by the SMA during its transformation from martensite to austenite and the SMA will likely recover all of its strain thus S=0. Or if the shell is very stiff, such as relatively thick steel, a very large force will be applied by the SMA to the shell during the transformation from martensite to austenite because the SMA is being restrained from recovering the strain, so we assume that the strain S is constant. What follows next is the development of equations to evaluate how the SMA ring segments will control unwanted external excitations by completing a forced response analysis via the modal expansion method and treating the SMA control forces applied to the cylindrical shell panel as an open loop system.

MODAL EXPANSION METHOD USED WITH OPEN LOOP SMA CONTROL FORCES

The modal expansion method is a means for evaluating the dynamic response for the shell deflections from the equations of motion via an infinite series of all participating modes each multiplied by a corresponding modal participation factor η_{mn} that determines the amount of effect each natural mode has on the total dynamic response. The general solution for the complete system response is shown in equation 13 (Soedel, 1981).

$$u_i(\alpha_1,\alpha_2,t)=\sum_{m=1}^{\infty}\sum_{n=1}^{\infty}\eta_{mn}(t)U_{imn}(\alpha_1,\alpha_2) \quad (13)$$

The subscript i = 1, 2, 3 refers to the in-plane and transverse directions, or i = x, ψ, 3 for the current reference directions used for the cylindrical shell panel in this analysis. The m and n subscripts refer to the m and n modes which are related to

the longitudinal and circumferential directions respectively. The U_{imn} are the mode shapes in the i directions for the (m,n) and the u_i are the total response for the shell deflections in the i directions. The modal participation factors are unknown and are determined from the following (Soedel, 1981)

$$\ddot{\eta}_{mn} + \frac{\lambda}{\rho h}\dot{\eta}_{mn} + \omega_{mn}^2 \eta_{mn} = F_{mn} \tag{14a}$$

$$F_{mn} = F_{mn}^m + F_{mn}^a \tag{14b}$$

The F_{mn}^a in this analysis is based on the SMA control force from the SMA ring segments and F_{mn}^m is based on other external loadings. The general form for F_{mn} with the loading only normal to the shell is defined as

$$F_{mn} = \frac{1}{\rho h N_{mn}} \int_{\alpha_1}\int_{\alpha_2} q_3 U_3 A_1 A_2 d\alpha_2 d\alpha_1 \tag{15}$$

$$N_{mn} = \int_{\alpha_1}\int_{\alpha_2} U_3^2 A_1 A_2 d\alpha_2 d\alpha_1 = \frac{RL\beta^*}{4} \tag{16}$$

λ is the damping ratio of the elastic shell, ρ is the mass density of the elastic shell, h is the shell thickness, ω_{mn} is the natural frequency for the (m,n) mode, and A_1 and A_2 are the Lamé parameters where $A_1 = A_x = 1$ and $A_2 = A_\psi = R$. For a simply supported cylindrical shell panel the mode shape function U_3 is

$$U_3 = C\sin\left(\frac{m\pi x}{L}\right)\sin\left(\frac{n\pi\psi}{\beta^*}\right) \tag{17}$$

In this analysis the limits of integration in equations 15 and 16 are from 0 to L in the x direction (α_1) and 0 to β^* in the ψ direction (α_2). The q_3^a represents a summation of forces from multiple SMA ring segments placed at different locations depending on the mode (m,n) and models them as line loadings along the circumference of the cylindrical shell panel. The Q_3 in the following equation for q_3^a comes from the terms in brackets that were mentioned as being labeled as Q_3 in the previous section. q_3^a is negative here because when the SMA ring segments constrict the forces from these actuators will be in the negative transverse (3) direction. The x_i^* represent the locations along the length of the shell where the SMA ring segments are to be placed and will vary depending on the mode which is to be controlled and N is the number or rings. **Figure 4** illustrates this configuration with N=2.

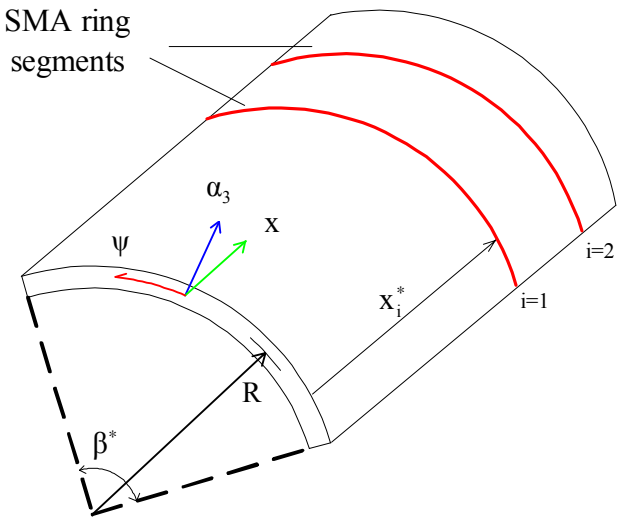

Figure 4 Cylindrical shell panel with SMA ring segments and notation defining their placement

Thus the total SMA actuation of N ring segments becomes

$$q_3^a = -\sum_{i=1}^{N} \frac{Q_3}{A_x}\delta\left(x - x_i^*\right) \tag{18}$$

Substitution of equations 16-18 into 15 gives

$$F_{mn}^a = -\frac{4}{\rho h RL\beta^*}\int_0^L\int_0^{\beta^*}\left[\sum_{i=1}^{N}\delta\left(x - x_i^*\right)\left[\frac{N_{\psi\psi}^a}{R} - \frac{1}{R^2}\frac{\partial^2 M_{\psi\psi}^a}{\partial\psi^2}\right]\cdot\sin\left(\frac{m\pi x}{L}\right)\sin\left(\frac{n\pi\psi}{\beta^*}\right)R\right]d\psi\,dx \tag{19}$$

Since $M_{\psi\psi}^a$ is not a function of ψ, the 2nd partial of $M_{\psi\psi}^a$ with respect to ψ will be zero. This reduces equation 19 to the following

$$F_{mn}^a = -\frac{4}{\rho h RL\beta^*}\int_0^L\int_0^{\beta^*}\left[\sum_{i=1}^{N}\delta\left(x - x_i^*\right)N_{\psi\psi}^a \cdot\sin\left(\frac{m\pi x}{L}\right)\sin\left(\frac{n\pi\psi}{\beta^*}\right)\right]d\psi\,dx \tag{20}$$

Integration along the length of the shell in the x direction from 0 to L yields

$$F_{mn}^a = -\frac{4N_{\psi\psi}^a}{\rho h RL\beta^*}\sum_{i=1}^{N}\sin\left(\frac{m\pi x_i^*}{L}\right)\int_0^{\beta^*}\sin\left(\frac{n\pi\psi}{\beta^*}\right)d\psi \tag{21}$$

After the final integration over the circumference of the shell from 0 to β^* equation 21 becomes

$$F_{mn}^{a} = \frac{4N_{\psi\psi}^{a}}{\rho hRL n\pi} \sum_{i=1}^{N} \sin\left(\frac{m\pi x_i^*}{L}\right) [\cos n\pi - 1] \qquad (22a)$$

where the last term in brackets shows that only the odd circumferential modes participate in the total response of the system.

$$[\cos(n\pi) - 1] = \begin{cases} -2 & n = 1, 3, 5, \ldots \\ 0 & n = 0, 2, 4, \ldots \end{cases} \qquad (22b)$$

This lends equation 22 to be written as

$$F_{mn}^{a} = -\frac{8N_{\psi\psi}^{a}}{\rho hRL n\pi} \sum_{i=1}^{N} \sin\left(\frac{m\pi x_i^*}{L}\right) \qquad n = 1, 3, 5, \ldots \qquad (23)$$

Now that F_{mn} for the SMA open loop control forces from the SMA ring segments has been evaluated, equation 14 can be solved for the modal participation factor to see the effect of the SMA control forces on the total system response; or additional forces from unwanted external excitations can be added to equation 14 with the SMA control forces to evaluate whether or not the SMA control forces can eliminate these disturbances by forcing the modal participation factor to zero. Such calculations are performed to solve for the modal participation factor via a FORTRAN program written by the author since a closed form solution could not be obtained because of the complexity of the martensite volume fraction. Heun's method, which is equivalent to a second order accurate Runge-Cutta scheme, is the algorithm used in the program to solve the system of differential equations (9 and 14) for the martensite volume fraction and the modal participation factor. These results are presented in the next section.

CONTROLLED RESPONSE OF CYLINDRICAL SHELL PANELS

The results presented in this section are based on the theoretical developments from the previous sections. All results presented here are based on the 90° cylindrical shell panel controlled by shape memory ring segments, the number depending on the mode (m,n), with the steel shell material properties and geometric dimensions listed in **Table 1** and the shape memory ring segments' material properties and geometry listed in **Table 2.** Before continuing it should be noted that the present shape memory alloys are not suitable for high-frequency applications. Though results presented here are performed using data from nickel-titanium (NiTi) shape memory alloys, this study is designed more for future shape memory material compositions that should have characteristics that are better suited to faster phase transformations and less hysteresis in regard to the martensite volume fraction (martensite and austenite finish temperatures much closer together). The method of heat transfer for this cylindrical shell panel and shape memory ring segment setup is also equally important and will likely require an efficient setup for heating and cooling in order to be applied to high frequency applications.

Table 1 Defining shell material properties and geometry

Cylindrical Shell Panel	Steel Material Properties and Shell Geometry
Elastic Modulus, Y	$30.0 \cdot 10^6$ psi
Mass Density, ρ	$7.35 \cdot 10^{-4}$ s^2 lb/in
Damping Ratio, ζ	0.02
Poisson's Ratio, μ	0.3
Curvature Angle, β^*	90°
Radius, R	1.9685 in
Length, L	3.937 in
shell thickness, h	0.03937 in

Table 2 Defining actuator material properties and geometry (Material properties taken from Dutta et al. 2004)

Shape Memory Ring Segments	Material Properties and Ring Geometry
Austenite Modulus, Y_A	5209580 psi
Martensite Modulus, Y_M	2970521 psi
mean +, m_+	78.9 °C
mean -, m_-	34 °C
standard deviation +, v_+	11.2 °C
standard deviation -, v_-	5.8 °C
initial strain, S_o	0.001
actuator width, w	0.125 in

As discussed previously, when using the modal participation expansion method to represent the complete response for the shell deflections, the goal is to reduce the modal oscillation to zero for each mode (m,n) via control forces to counter the unwanted external excitations. These results generated here are used to show how the SMA ring segments can control the (m,n) modes based on a sinusoidal external excitation. This requires an input shaping technique and in some cases minor tuning with respect to the phase or frequency of input because a sinusoidal temperature input to the SMA does not result in a sinusoidal force response and they do not line up exactly out of phase, hence no exact cancellation with the unwanted sinusoidal external excitation. The following results show various temperature input functions with appropriate phase shift applied to the SMA ring segments to achieve a certain level of cancellation with the sinusoidal external excitation. Aside from the sinusoidal

temperature input originally planned to control the SMA ring segments, a saw tooth wave is tried and several different waveforms created by using a Fourier analysis applied to multiple exponential functions are also in development but not presented here.

Originally a sinusoidal function for the temperature input to the SMA had been chosen to control the shape memory alloy's actuation in response to an external sinusoidal excitation. The specifications for this function are based on assuming the SMA is initially in the martensite phase and will take advantage of the full range of the given shape memory alloy's material properties, i.e., the SMA will be heated and cooled just above and below the austenite and martensite finish temperatures respectively. For the material properties of the NiTi SMA used, this means that the SMA is to be heated and cooled between 15 and 115°C. With these specifications the temperature input function is given by equation 24.

$$\theta(t) = 50\cos(\omega t + \pi) + 65 \tag{24}$$

θ represents temperature (units of Celsius are used throughout), t represents time, and ω, the frequency (rad/s), is chosen to match the frequency of the external excitation, but in some cases it is tuned or the phase shift is changed to make the SMA response more synchronous with the external excitation.

The sinusoidal external excitation used here is a uniform pressure loading, but other types of loadings could be used depending on the conditions, such as concentrated point and line loadings. For the forced vibration analysis using the modal expansion method this external excitation can be represented as:

$$F_{mn} = \frac{1}{\rho h N_{mn}} \int_{\alpha_1} \int_{\alpha_2} q_3 U_3 A_1 A_2 d\alpha_2 d\alpha_1 \tag{25a}$$

$$N_{mn} = \int_{\alpha_1} \int_{\alpha_2} U_3^2 A_1 A_2 d\alpha_2 d\alpha_1 = \frac{RL\beta^*}{4} \tag{25b}$$

where the q_3 used here represents an external mechanical loading, uniform pressure here, like the q_3^a used previously to represent the control force induced by the SMA actuator. Since the external pressure loading is sinusoidal it can be represented as:

$$q_3 = P_1\cos(\omega t) + P_2 \tag{26}$$

where P_1 and P_2 are constant values to determine amplitude and position above or below the x-axis (time) respectively. After integration over the cylindrical shell panel surface the external loading F_{mn}^m from equation 25a can be represented as:

$$F_{mn}^m = \frac{16q_3}{\rho h m n \pi^2} \qquad \begin{matrix} m = 1, 3, 5, \ldots \\ n = 1, 3, 5, \ldots \end{matrix} \tag{27}$$

Note that this type of loading only affects the odd modes circumferentially and longitudinally. This is good since in the previous section it was found that for the circumferential modes only the odd ones can be controlled, at least in the current configuration, but if the SMA ring segments are segmented again such that there are 2 segments for n=2 and four for n=4 and so on as opposed to the original single segment traversing the full circumferential length of the cylindrical shell panel. **Figure 5a** shows the applied uniform sinusoidal pressure loading, equations 26 and 27, and the response of the modal participation factor η to this loading alone for the (1,1) mode and ω=500 rad/s, and the natural frequency for the elastic shell is ω_{1mn} = 35330.19 rad/s or f_{1mn} = 5622.9794 Hz. **Figure 5b** is used as the standard response compared with the various SMA input waveforms discussed later. As discussed previously the current shape memory alloys are not suitable for high frequency applications, therefore this investigation applies to future shape memory alloy compositions and an efficient heat transfer setup.

External loading freq. ω (rad/s)	Shell 1st natural freq. ω_{1mn} (rad/s)	Shell 1st natural freq. f_{1mn} (Hz)
500	35330.2	5622.974

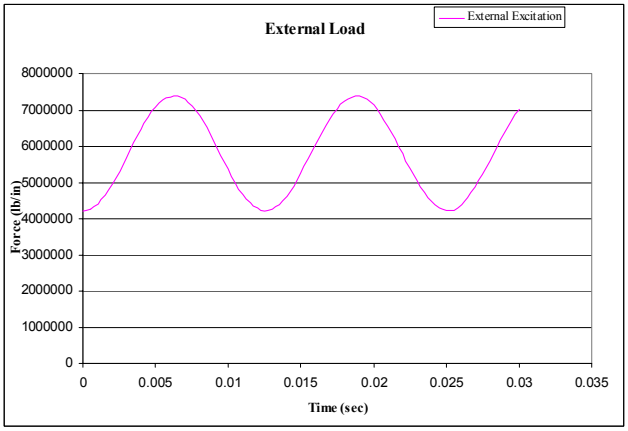

(a) Uniform sinusoidal pressure loading from equation 6.3.7

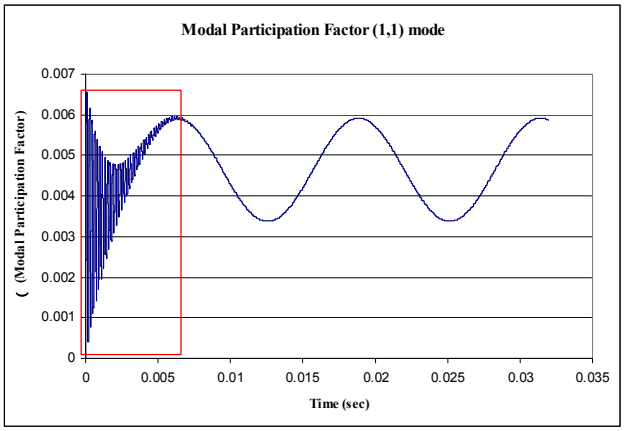

(b) Modal participation factor response to loading in **(a)**

Figure 5 Applied sinusoidal loading and modal participation factor response (1,1) mode

As expected from **Figure 5b** it can be seen that at steady state the response of the modal participation factor resembles the applied loading. The high frequency oscillatory transient behavior seen at the beginning of Figure **5b,** enclosed by the red box, is defined by the cylindrical shell panel 1st natural frequency. The following temperature input waveforms in the next sections to be tested include regular sinusoids with phase shift in some cases, and a saw tooth wave with phase shift. Variations on piecewise exponential functions transformed to Fourier series' used as the temperature input for better reduction of the modal oscillation amplitude to zero are planned to be used later and the results will be presented in a future paper. For the following figures of various test cases, **6-8**, **(a)** illustrates the waveform used as the temperature input, **(b)** shows the response of the martensite volume fraction to the waveform input in part **(a)**, **(c)** illustrates the external sinusoidal loading and SMA actuation force, and **(d)** shows the controlled modal response.

Case 1: Sinusoidal Waveform

The following **Figures 6** and **7** show results from a sinusoidal temperature waveform input to the SMA actuators, recall that the parts to each figure are **(a)** the waveform of temperature input, **(b)** the martensite volume fraction response, **(c)** the applied loadings (including both sinusoidal external loading and SMA actuation force, and **(d)** the response of the modal participation factor to both the uniform sinusoidal external excitation and the control force induced by the SMA actuator. Assuming the external sinusoidal load advances by a phase shift of $\pi/8$ as seen in **Figure 7,** there is better cancellation of the modal participation factor. Note that there is a transient behavior at the beginning of the modal participation factor response in **Figure 7d,** enclosed by red box, but not in **Figure 6d**. This appears to be caused by the phase shift applied to the external loading since there is no exact cancellation between the external loading and the SMA control force at the beginning, as seen in Figure **7c,** while there is exact cancellation at the beginning in **Figure 6c**. Unfortunately only so much can be done with changing the phase shift to help cancellation of the modal participation factor, which leads to the use of other temperature input functions to the SMA since a sinusoidal temperature input does not yield a sinusoidal response from the SMA control force as seen in **Figures 6c** and **7c**.

SMA actuation freq. ω (rad/s)	External loading freq. ω (rad/s)	Shell 1st natural freq. ω_{1mn} (rad/s)	Shell 1st natural freq. f_{1mn} (Hz)
500	500	35330.2	5622.974

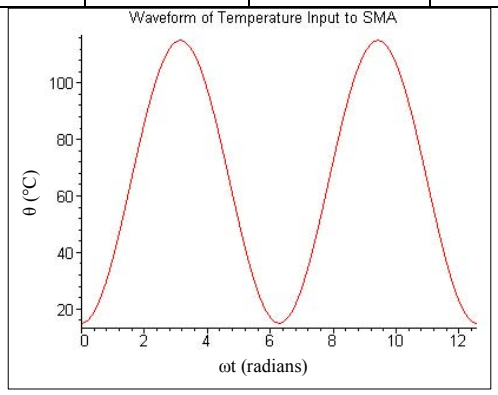

(a) Sinusoidal waveform of temperature input to SMA

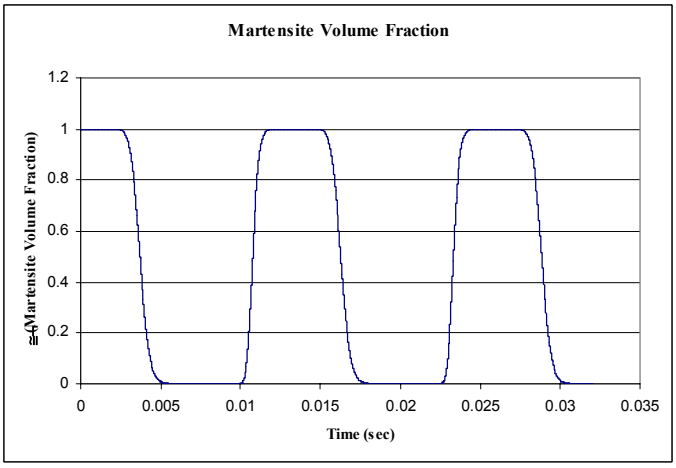

(b) Martensite Volume fraction response to the temperature input

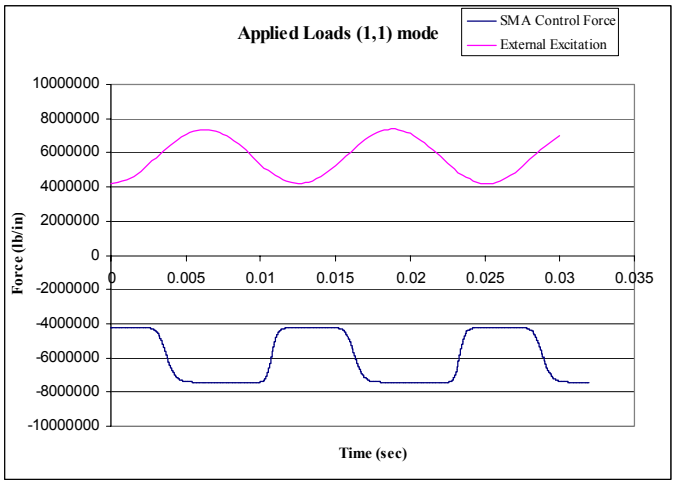

(c) Applied loadings (including both external sinusoidal loading and SMA control force) to cylindrical shell panel

Figure 6 Controlled response of system for (1,1) mode

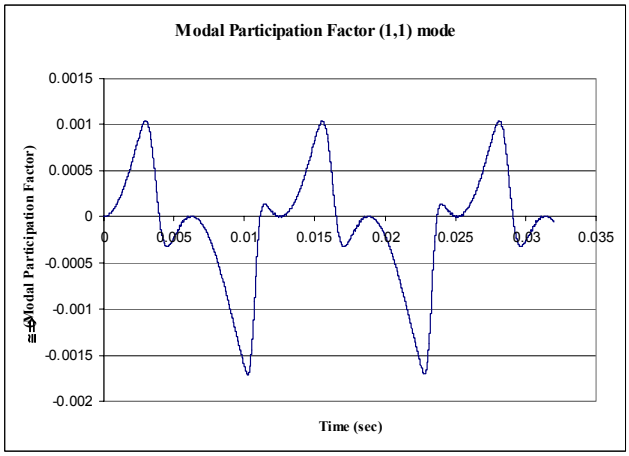

(c) Response of modal participation factor to applied loadings in **(c)**

Figure 6 (continued) Controlled response of system for (1,1) mode

SMA actuation freq. ω (rad/s)	External loading freq. ω (rad/s)	External loading phase shift (rad)	Shell 1st natural freq. ω_{1mn} (rad/s)	Shell 1st natural freq. f_{1mn} (Hz)
500	500	π/8	35330.19	5622.974

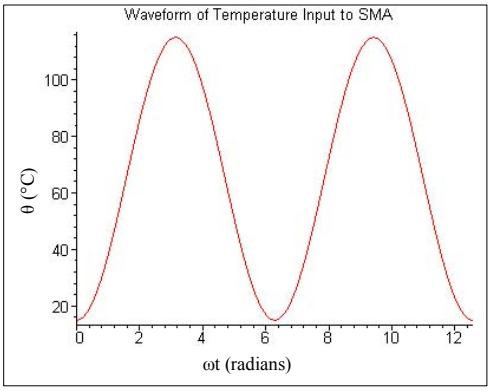

(a) Sinusoidal waveform of temperature input to SMA

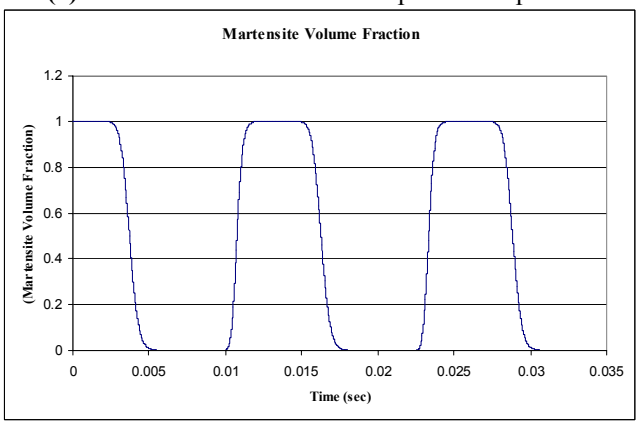

(b) Martensite Volume fraction response to the temperature input

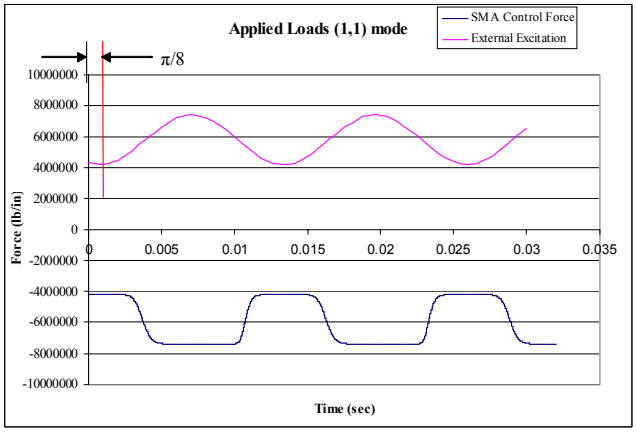

(c) Applied loadings (including both external sinusoidal loading and SMA control force) to cylindrical shell panel

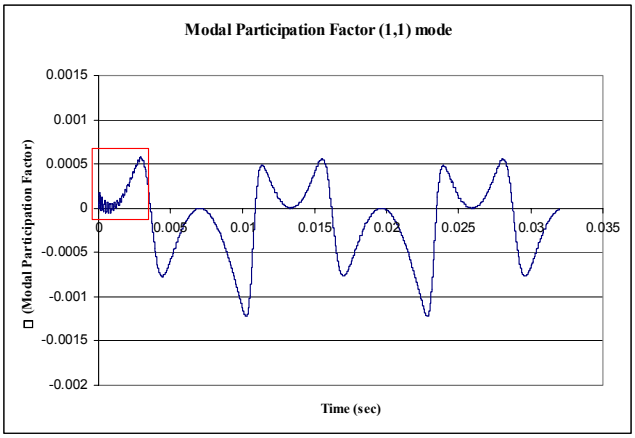

(d) Response of modal participation factor to applied loadings in **(c)**

Figure 7 Controlled response of system for (1,1) mode

Since using a sinusoidal function for temperature input to the SMA with proper phase shift tuning is not adequate enough to eliminate the response of the modal participation factor to an external sinusoidal uniform pressure loading, another temperature input function is tested here to see what will work the best. A saw-tooth waveform for temperature input is tried and as discussed previously some temperature input waveforms created by piecing together exponential functions which are then combined into a single function from a truncated Fourier series based on those functions over a limited range will be used and the results presented in another paper.

Case 2: Saw-tooth Waveform

The saw-tooth waveform for temperature input is shown in the next equation. The H_o=65 refers to the average value of the waveform and H=50 is the amplitude.

$$\theta(t) = H_o - \sum_{\ell=1}^{\infty} \frac{8H}{\pi^2} \frac{1}{(2\ell-1)^2} \cos((2\ell-1)\omega t) \qquad (28)$$

Figure 8a illustrates the saw-tooth temperature input waveform, **Figure 8b** gives the martensite volume fraction response to this input, **Figure 8c** shows the applied loads including the external sinusoidal pressure loading and the SMA control force, and **Figure 8d** shows the response of the modal participation factor to the external sinusoidal uniform pressure loading and the control force induced by the SMA with the saw-tooth waveform of equation 28 and phase advance of π/6 used as the temperature input to the SMA. The results are a little better than the sinusoid temperature inputs but not significant enough to warrant further use. Again, the transient high frequency shell oscillation is observed in **Figure 8d,** enclosed by the red box.

SMA actuation freq. ω (rad/s)	External loading freq. ω (rad/s)	External loading phase shift (rad)	Shell 1st natural freq. ω_{1mn} (rad/s)	Shell 1st natural freq. f_{1mn} (Hz)
500	500	π/6	35330.19	5622.974

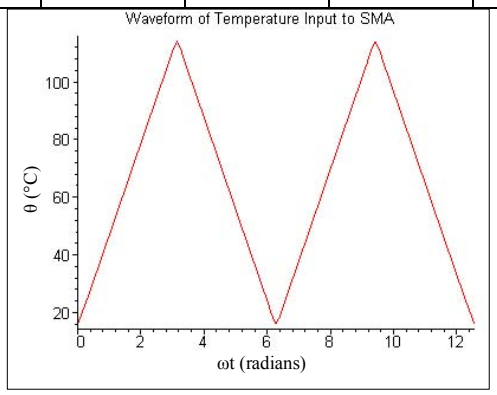

(a) Saw tooth waveform of temperature input to SMA

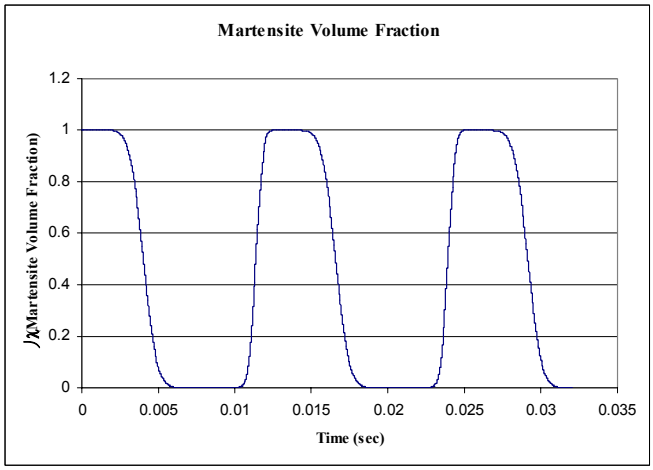

(b) Martensite Volume fraction response to the temperature input

Figure 8 Controlled response of system for (1,1) mode

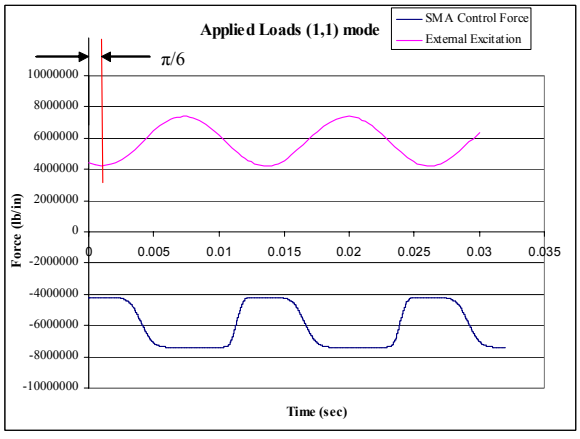

(c) Applied loadings (including both external sinusoidal loading and SMA control force) to cylindrical shell panel

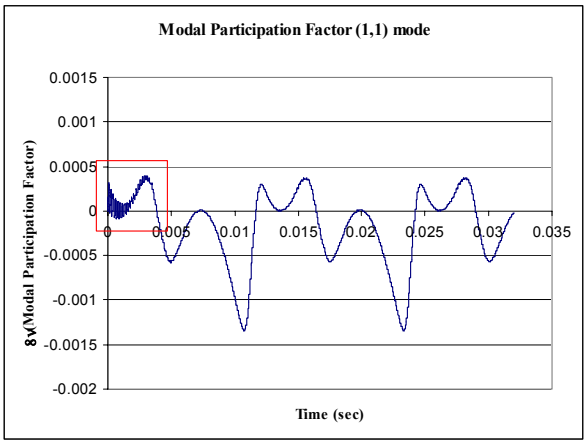

(d) Response of modal participation factor to applied loadings in **(c)**

Figure 8 (continued) Controlled response of system for (1,1) mode

Table 3 gives a summary of the waveforms for temperature input to the SMA ring segments. Recall that all functions exploit full range of SMA martensite and austenite transformations (heating from 15°C to 115°C and then back to 15°C for one complete cycle of the SMA); and the unwanted external excitation in every case is a sinusoidal uniform pressure loading applied to the cylindrical shell panel. The last column gives the reduction percentage of modal oscillation amplitude, which is reduced by the SMA for each given temperature input by comparing this new response to the original modal participation factor response from the external excitation alone.

Table 3 Controlled responses from various temperature input functions

Waveform	SMA actuation freq. ω (rad/s)	Shell 1st natural freq. ω_{1mn} (rad/s)	External loading phase shift (rad)	Reduction % of modal response
sinusoidal	500	35330.19	0	-7.9
sinusoidal	500	35330.19	$\pi/8$	30.2
saw tooth	500	35330.19	$\pi/6$	32.9

The results from **Figures 6-8** and **Table 3** show that the SMA ring segments are capable, to a certain extent, of controlling unwanted vibrations affecting cylindrical shell panels. For a sinusoidal pressure loading as the unwanted vibration, a sinusoidal temperature input with appropriate phase shift can be used as temperature input to the SMA for controlling the unwanted vibration, but the SMA actuators could be more effective with the appropriate input since the current response to a sinusoidal input is more like a square wave than a sine wave. A saw tooth wave for temperature input showed a little better results but not significantly greater than the sinusoidal temperature input. Currently other waveforms based on piecewise exponential functions and considering the martensite volume fraction response to temperature are being tested and the results from that analysis will be presented in a future paper.

CONCLUSIONS

The equations of motion and mode shape functions for a simply supported cylindrical shell panel were given and used to determine how the forces from the SMA ring segments can be represented in terms of N_{ij} and M_{ij}, the membrane force per unit length and the bending moment per unit length respectively. With these expressions, and making the inclusion of the ability to incorporate multiple SMA rings segments with their placement determined by the mode number (m,n), the open loop control forces of the SMA ring segments were determined from the modal expansion method. In order to test the ability of these SMA actuators to control unwanted external vibrations, a sinusoidal pressure loading was used as the unwanted vibration and the force from the SMA actuators was applied with sinusoidal and saw tooth temperature input waveforms. With appropriate phase shift applied to these functions the SMA actuators were capable of controlling the vibration but not by a significant amount. This is because the SMA force response to a sinusoidal temperature input is not sinusoidal. Choosing other waveforms for temperature input such as the saw tooth waveform, give more promising results in an attempt to find an input waveform to the SMA that will yield a sinusoidal response for the SMA force generated by the ring segments. Other waveforms are under consideration and testing, such as piecewise exponentials.

ACKNOWLEDGMENTS

This research is supported, in part, by a grant from the NASA-Glenn Research Center, Program Managers: S.M. Arnolds and H.-J. Lee. This support is gratefully acknowledged.

REFERENCES

Baz, A., Chen, T., and Ro, J., 2000, "Shape Control of NITINOL-reinforced Composite Beams," *Composites Part B: Engineering*, Vol. 31, pp. 631-642.

Buehler, W. J., Gilfrich, J. V., and Wiley, R. C., 1963, "Effect of Low-Temperature Phase Change on the Mechanical Properties of Alloys Near Composition TiNi," *Journal of Applied Physics*, Vol. 34, pp. 1475-1477.

Chang, L. C. and Read, T. A., 1951, "Plastic Deformation and Diffusionless Phase Change in Metals-the Gold-Cadmium Beta Phase," *Transactions AIME J. Met.*, Vol. 191, pp. 47-52.

Chen, T., Ruzzene, M., and Baz, A., 2000, "Control of Wave Propagation in Composite Rods Using Shape Memory Inserts: Theory and Experiments," *Journal of Vibration and Control*, Vol. 6, pp. 1065-1081.

DeHaven, J.G., and Tzou, H.S., 2005, "Transition of Neural Signals on Cylindrical Shells with Various Curvatures," *Proceedings of IDETC/CIE 2005, ASME 2005 International Design Engineering Technical Conferences & Computers and Information in Engineering Conference*, Long Beach, California, USA, September 24-28, 2005. (Paper No. DETC2005-85153)

Dutta, S. M., Ghorbel, F. H., and Dabney, J. B., 2004, "Dynamic Modeling and Control of Hysteresis in a Shape Memory Alloy Actuator," *Proceedings of IMECE04, 2004 ASME International Mechanical Engineering Congress and Exposition,* Anaheim, California USA, November 13-20, 2004. (Paper No. IMECE2004-61849)

Jia, J. and Rogers, C. A., 1990, "Formulation of a Laminated Shell Theory Incorporating Embedded Distributed Actuators," Transactions of ASME, Vol. 112, pp. 596-604.

Kudva, J. N., Appa, K., Martin, C. A., Jardine, A. P., Sendeckyi, G., Harris, T., McGowan, A., and Lake, R., 1997, "Design, Fabrication, and Testing of the DARPA / Wright Lab 'Smart Wing' Wind Tunnel Model," AIAA Paper 97-1198, April 1997.

Lattime, S. B. and Steinetz, B. M., 2002, "Turbine Engine Clearance Control Systems: Current Practices and Future Directions," AIAA Paper 2002-3790, September 2002.

Lee, J. L., and Lee, J. J., 2000, "Evaluation of the

characteristics of a shape memory alloy spring actuator," *Smart Materials and Structures*, Vol. 9, pp. 817-823.

Ma, N., Song, G., and Lee, H. J., 2003, "Position Control of SMA Actuators with Internal Electrical Resistance Feedback," *Smart Structures and Materials*, Vol. 5049, pp. 46-54.

Madill, D. R., and Wang, D., 1998, "Modeling and L-2 Stability of a Shape Memory Alloy Position Control System," *IEEE Transactions on Control Systems Technology*, Vol. 6, No. 4, pp. 473-481.

Mineta, T., Mitsui, T., Watanabe, Y., Kobayashi, S., Haga, Y., and Esashi, M., 2002, "An Active Guide Wire with Shape Memory Alloy Bending Actuator Fabricated by Room Temperature Process," *Sensors and Actuators A*, Vol. 97-98, pp. 632-637.

Paine, J. S. N., Rogers, C. A., and Smith, R. A., 1995, "Adaptive Composite Materials with Shape Memory Alloy Actuators for Cylinders and Pressure Vessels," *Journal of Intelligent Material Systems and Structures*, Vol. 6, pp. 210-219.

Rediniotis, O. K., Lagoudas, D. C., Garner, L. J., and Wilson, N., 1998, "Experiments and Analysis of an Active Hydrofoil with SMA Actuators," *AIAA Paper: AIAA-98-0102 presented at the 36th Aerospace Sciences Meeting and Exhibit, Reno, NV, January 12-15*.

Soedel, W., 1981, *Vibration of Shells and Plates*, Marcel Dekker, Inc., New York and Basel.

Schetky, M., and Steinetz, B. M., 1998, "Shape Memory Alloy Adaptive Control of Gas Turbine Engine Compressor Blade Tip Clearance," *Smart Structures and Materials*, Vol. 3326, pp. 346-354.

Tzou, H.S., 1993, *Piezoelectric Shells-Distributed Sensing and Control of Continua* Kluwer Academic Publishers, Boston/Dordrecht.